International Journal on Advanced Science Engineering Information Technology

Vol.10 (2020) No. 6
ISSN: 2088-5334

Development of a New Polymer Membrane: *Polyvinylidene fluoride/Polyetherimide* Blend Membrane

Nita Kusumawati[a,1], Agus Budi Santoso[b], Setya Chendra Wibawa[c], Pirim Setiarso[a], Supari Muslim[b,2]

[a] *Department of Chemistry, Universitas Negeri Surabaya, Ketintang, Surabaya, 60231, Indonesia*
E-mail: [1]nkusumawati82@yahoo.com

[b] *Department of Electrical Engineering, Universitas Negeri Surabaya, Ketintang, Surabaya, 60231, Indonesia*
E-mail: [1]suparimuslim@gmail.com

[c] *Department of Information Engineering, Universitas Negeri Surabaya, Ketintang, Surabaya, 60231, Indonesia*
E-mail: setyachendra@unesa.ac.id

Abstract*— *Porous polyetherimide (PEI)/polyvinylidene fluoride (PVDF)* coated flat sheet membranes with different compositions and polyethene glycol (PEG) *pyrogenic* additives have been prepared by non-solvent induced phase separation for the separation of metal salts and sucrose. By using non-solvent induction phase separation (NIPS), it has succeeded in preparing new members of mixed matrix PVDF membrane with (i) asymmetry pore structure, (ii) porosity 7.19%-18.93%, (iii) pore size 0.196 nm-0.453 nm and (iv) mechanical strength 4262.04-24472.57 N/m^2, (vi) permeability respectively of 500.48 L/m^2.h.bar for $C_{12}H_{22}O_{11}$; 642.94 L/m^2.h.bar for NaCl; 623.64 L/m^2.h.bar for $MgCl_2$; 1060.39 L/m^2.h.bar for $CaCl_2$; and 1292.85 L/m^2.h.bar for $CuSO_4$. Specifically, increasing PEI levels up to 2(wt.%) - 8 (wt.%) has reduced overall porosity and pore size, thus having a specific impact on mechanical strength, pure water permeability (PWF) and the permeability of the feed solution. The opposite phenomenon is observed when the PEI level reaches 10 (wt.%) - 14 (wt.%). Furthermore, compared to pure PEI membranes, PVDF/PEI composite membranes were observed to have a higher resistance to acids and lower to bases. This condition applies in contrast to pure PVDF membranes. Despite having moderate chemical resistance, PEI/PVDF membranes have excellent characteristics and separation performance compared to pure membranes. This demonstrates its promising potential for separation of soluble metal salts and sucrose produced by various industrial processes compared to PVDF and PEI membranes.

***Keywords*— membrane; polyvinylidene fluoride; polyetherimide; soluble metal salt; sucrose.**

I. INTRODUCTION

The world faces major challenges in the fulfilment of the increasing demand for primary components in human life (water, energy, food and other essential ingredients) in addition to demands for the reduction and minimization of the negative impacts of human activity on a global scale and full attention to climate change on Earth [1]–[5]. Major advances in chemistry, engineering, and sustainable materials (SusChEM) create great opportunities in overcoming global challenges and demands on the presence of primary components that are increasingly depleted and potentially life-threatening. In recent years membrane technology has attracted much of the world attention in dealing with a number of crucial problems that are directly related to the increasing difficulty level of access to these primary components [6]. Polymer membranes have become an essential part of various applications related to sustainability because of the selective separation properties [7]–[9] and no additional chemical required in the process. The *polyvinyl fluoride* (PVDF) membrane is a major commercial microfiltration membrane that is widely used in many applications in industry, especially because of its advantages compared to many other organic polymeric materials, including high thermal and chemical resistance. In addition, PVDF membrane has high mechanical strength and asymmetry structure required for separation [10]–[12].

Polyetherimide (PEI) is an amorphous polymer [13], [14] which capable to forming a membrane with an asymmetry structure, in which its surface morphology is predominantly dominated by high porosities and accompanied by a low thickness of the cross-sectional structure. This typical morphology has caused the PEI membrane to tend to produce high permeability. High pore quantity and low membrane thickness have been a compensatory factor for the homogeneous pore of the PEI membrane as well as better induction of membrane mechanical resistance. In addition,

PEI has high chemical and thermal stability (± 500 ˚C) [15], [16]. Despite having higher thermal stability than PVDF, the chemical resistance of the PEI membrane lies below the PVDF membrane. The PEI membrane tends to have weak resistance in acidic environments while PVDF in strong alkaline. However, low wettability by polar compound due to the hydrophobic surface and low surface energy and lower heat resistance due to its lower melting point begins to limit the application of PVDF membranes to specific processes involving thermal and mechanical capabilities in the industry [7]–[11], [17]. Thus, a combination of advantages and disadvantages of PEI and PVDF becomes a potential step to resolve such limitations.

One viable alternative to fix this weakness is the modification of the PVDF membrane using the PEI polymer to produce a composite membrane with better hydrophilic properties. From the various modification methods available in the literature, blending using polymeric materials that have targeted properties, is a simple and effective choice [15], [18]. In recent years, mixed matrix membranes (MMMs) have gained much attention because of their advantages which can provide many functions as multifunctional membranes that support SusChEM with enhanced properties and performance [2], [19]–[22]. The blending particles distributed homogeneously and change the overall properties of the membrane. The quality and quantity of the blending are determined by several factors such as the composition of the dope solution, temperature, type of polymer material, also solvents and additives [23]–[26]. However, the most important determinant parameter is the time between casting and immersion in the coagulation bath because PEI can only migrate in the solution phase. This time can be modified, shortened or extended as needed, on flat sheet membrane casting process [27], [28].

In previous studies, the effects of PVDF addition on the characteristics of PSf/PVDF composite membranes have been studied [7]–[11]. The results show that the physical morphology, mechanical strength also thermal dan chemical resistant of the composite membrane, are strongly influenced by the concentration of PVDF in the blending solution which migration is found to occur at a limited level however the hydrophobic membrane properties are slightly elevated. PVDF has a high fluorine content (59.4% by weight) that control the hydrophobic properties of the blended membrane [29]–[31]. In this regard, it would be a potential choice if it then applied these results to obtain an opposite yield in this research, i.e. the improvement of the hydrophobic nature of the PVDF membrane using a more hydrophilic PEI polymer [32].

The purpose of this study was to examine the effect of PVDF modification with PEI polymer performed by blending method on the properties and performance of flat-sheet composite membranes in the separation of dissolved metal salts and sucrose. In this study, the PEI levels added to the PVDF polymer solution were changed while the levels of PVDF, NMP solvents and PEG additives were made constant, and the effect was also studied. It should be noted that different membrane physical characteristics such as porosity, pore size and tortuosity as well as mechanical, thermal and chemical resistance of membranes affect the performance of membranes in specific applications in complex ways. Related to this, the reduction of the hydrophobic properties of the membrane obtained from the blending of PVDF and PEI polymer solution is only one of the factors that determine membrane performance.

The blending method affects the phase separation phenomenon, where an increase in the viscosity of the resulting polymer solution reduces the level of non-solvent penetration. This condition minimizes the disruption to the thermodynamic equilibrium of the casting solution and induces delayed liquid-liquid demixing in the phase separation process.

II. Material and Method

A. Material

Non-woven fabric 254 mesh used as a supporting layer purchased from PT. Kasa Husada Wira Jatim (Indonesia). The powdered PVDF polymer with an average molecular weight of 534,000 is provided by Aldrich (Singapore). PEI in pellet form is purchased from Aldrich (Singapore). All these polymer materials are used directly without preceding drying at a specific temperature and time. N-methyl-2-pyrrolidone (NMP) grade biotech with a purity of ≥99.7%) was purchased from Aldrich (Singapore) and also used directly without further examination. Polyethene glycol (PEG-6000) with a purity level of ≥ 99.5%, used as a pore-forming additive purchased from PT. Bratachem (China).

B. PVDF/PEI Membrane Preparation

For the preparation of casting solutions each 12 g of PVDF; 2 g of PEI; and 2 g of PEG-6000 were added to 84 g of NMP solvent. Furthermore, in order to optimize the solubility, 7 h of stirring was performed using NESCO LAB MS-H280-Pro magnetic stirrer at 60 °C. In the next step, it has been done ageing of the casting solution for 18 h at room temperature in order to obtain a bubble-free casting solution. The air bubbles presence generally results in membrane defects. The casting solution preparation follows the composition, as shown in Table I. Compositions M1 and M7 are used as a control/comparison for the properties and performance of M2-M7 composite membranes resulted.

TABLE I
Composition of The Blending Solution

Membrane	PVDF (wt.%)	PEI (wt.%)	PEG-6000 (wt.%)	NMP (wt.%)
M1	14	0	2	84
M2	12	2	2	84
M3	10	4	2	84
M4	8	6	2	84
M5	6	8	2	84
M6	4	10	2	84
M7	2	12	2	84
M8	0	14	2	84

PVDF/PEI composite membranes are made using the NIPS method. The blended solution is cast on a glass sheet coated with a gauze support layer. The casting is done by casting knife at 40 °C with 800 μm thickness. After ageing for 30 minutes at the same temperature, the subsequent casting solution is immersed in a coagulation medium

containing distilled water at 40 °C for 2 h to induce phase separation. To remove residual solvents and pyrogen additives still attached to the membrane, a membrane was immersed in distilled water for 24 hours. Membrane dried in the open air for 24 hours and ready to be analyzed.

C. PVDF/PEI Characterization

1) Scanning Electron Microscope (SEM): Zeiss EVO MA10 analyzed surface and cross-section morphology of (1) PVDF membrane, (2) PVDF/PEI composite membrane, and (3) PEI membrane. Dry membranes were broken in liquid nitrogen and coated with gold by sputtering before each analysis. The upper surface of the cross-sectional image is the skin layer (the membrane side that is in direct contact with the non-solvent), while the lower surface is a porous layer generally composed of *micropores* and *microvoids*. Morphological analysis using SEM was performed at 200 kV acceleration [33].

2) Fourier Transform Infra-Red (FTIR): The infrared spectra of the membrane were analyzed by Nicolet IS10 Thermo Scientific FTIR spectrophotometer in the range of 4,000-400 cm^{-1}. Through this functional group analysis, blending PVDF and PEI are confirmed.

3) Porosimeter and Pore Size Analysis: Membrane porosity was measured by dry-wet weight method. After the dry weight was weighed, the membranes were immersed in deionized water for 24 hours to optimize water penetration into the membrane pores. Once the excess water on the membrane surface was removed using tissue paper, the wet weight of the membrane was weighed. Membrane porosity was analyzed using the following equation [10], [34].

$$P(\%) = \frac{W_w - W_d}{\rho_w \, x \, A \, x \, \delta} \, x \, 100 \qquad (1)$$

Where m_w is the wet weight (g) of the membrane, m_d is the dry weight (g) of the membrane, ρ_w is the pure water density (g/cm^3) at 25 ˚C, A is the thickness of the wet (cm) membrane. To reduce the level of experimental error, the resulting porosity is the average result of three times measurement.

The membrane pore radius (r_m) was analyzed using the *Guerout-Elford-Ferry* equation, as shown in equation 2.

$$r_m = \sqrt{\frac{(2.9 - 1.75\varepsilon) x \, 8\eta l Q}{\varepsilon \, x \, A \, x \, \Delta P}} \qquad (2)$$

Where η is the deionized water viscosity (8,9 x 10^{-4} Pa.s); Q is the permeate volume per unit time (m^3/s), and ΔP is the operational pressure of separation (0.1 MPa).

4) Mechanical Strength: The mechanical membrane characterization was performed using RCT-10KN-AF Toyo Seiki Stereograph. All membranes to be tested were dried at a temperature of 30 ˚C overnight before the cut to size 15 mm x 100 mm. Clipping distance is kept constant at 50 mm. Measurements were made at room temperature, and strain rate of 20 mm/min was applied. Young's modulus value generated was an average of the three times measurement. The Young's modulus (E) was calculated according to Equation 3 [10]:

$$E = \frac{Stress}{Strain} \qquad (3)$$

Where the stress is the force acting per area of material (Nm^{-2}), and strain represents the ratio of the length increase to the initial length. To reduce experimental error, the reported Young's modulus is the average of the three times measurement.

5) Flux Test and Filtration Experiment: Filtrations were evaluated using the "Dead end" membrane reactor (self-made), at room temperature and pressure of 1 bar. The membrane samples were placed in the reactor and sealed with an O-ring. The membrane area tested was 0.00246176 m^2. The feed volume used was 250 mL. Permeation ($l/m^2h.bar$), determined by the gravimetric method. Pure water, as well as soluble metal salts and sucrose flux (Lm-2h-1), was determined using Equation 4 [11].

$$J = \frac{V}{A \times t} \qquad (4)$$

Where V is the volume of the feed solution (L), A is the membrane surface area (m^2), and t is the time required by the feed solution to pass through the membrane (h).

6) Thermal Resistance: The thermal resistance of the membranes was evaluated using Perkin Elmer STA-6000 Differential Scanning Calorimetry (DSC) - Thermal Gravimetry Analysis (TGA) with heating temperature range 20 ºC - 700 ºC with 10 ºC min^{-1} a heating rate.

7) Chemical Resistance: Membrane acid resistance was determined by immersion in 80 vol% sulfuric acid solution, while alkaline resistance was determined by immersion in 80 wt.% sodium hydroxide. Changes in functional groups before and after treatment were analyzed with FTIR spectrophotometer. The results show the functional groups are lost after treatment.

III. Results and Discussion

A. Physical Characterization of the Membrane

Fig. 1 shows the pure PVDF, PVDF/PEI composite, and pure PEI membrane surface morphology. Differences were observed in surface and cross-section morphology of PVDF/PEI membranes compared to pure PVDF and PEI membranes. This difference is increasingly significant with increasing PEI levels. As shown in Fig. 1 (a1) and (e1), the surface of pure PVDF membrane has a higher porosity with smaller pore size than PEI membrane. To further evaluate the composite membrane structure, a morphological analysis of the cross-section of the composite membrane was carried out. The results of the morphological analysis of the membrane cross-section are shown in Fig 2. The figure shows the M7 and M8 membranes structure with high porosity typical of PEI membranes. This visual is different from the results of the surface morphological analysis, which shows low porosity with large pore size. This shows the different pores types that make up the skin and porous layer.

In this case, porosity and pore size (see Table II) are the determining parameters for overall pore characteristics. Compared with PEI membranes, lower porosity and pore size were observed on pure PVDF membranes. The narrower pore size distribution on pure PVDF membranes is predicted to be the determinant of this characteristic.

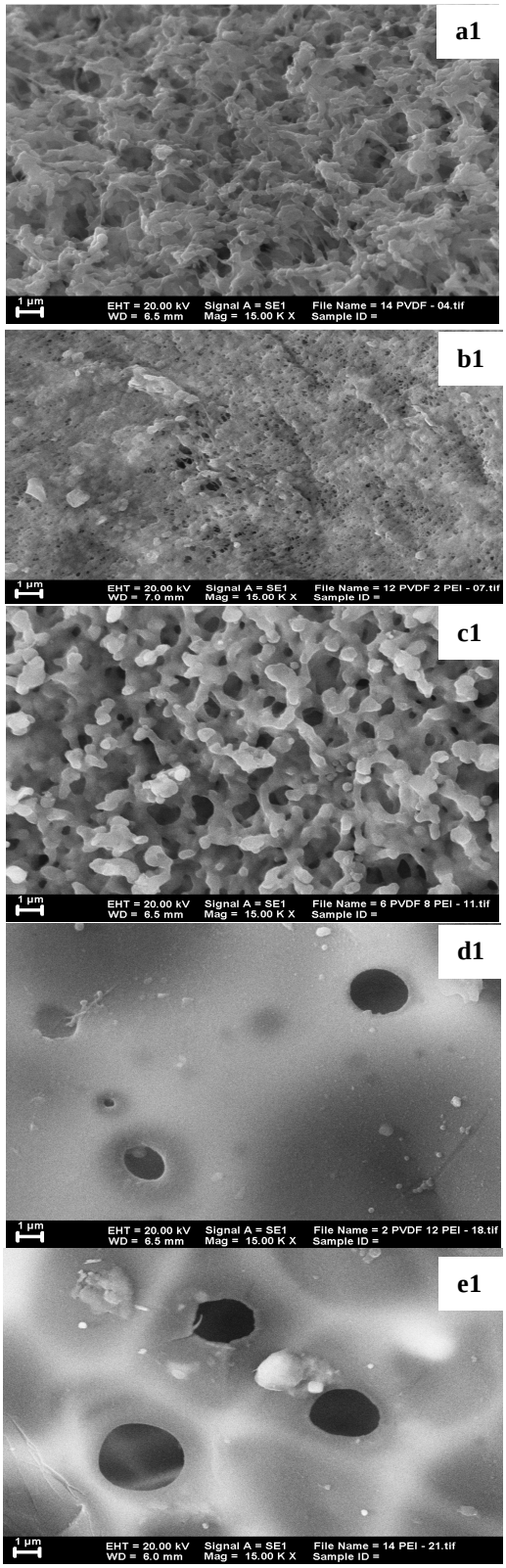

Fig. 1 SEM images of the surface morphologies of the M1 (a1), M2 (b1), M5 (c1), M7 (d1), and M8 (e1) membrane

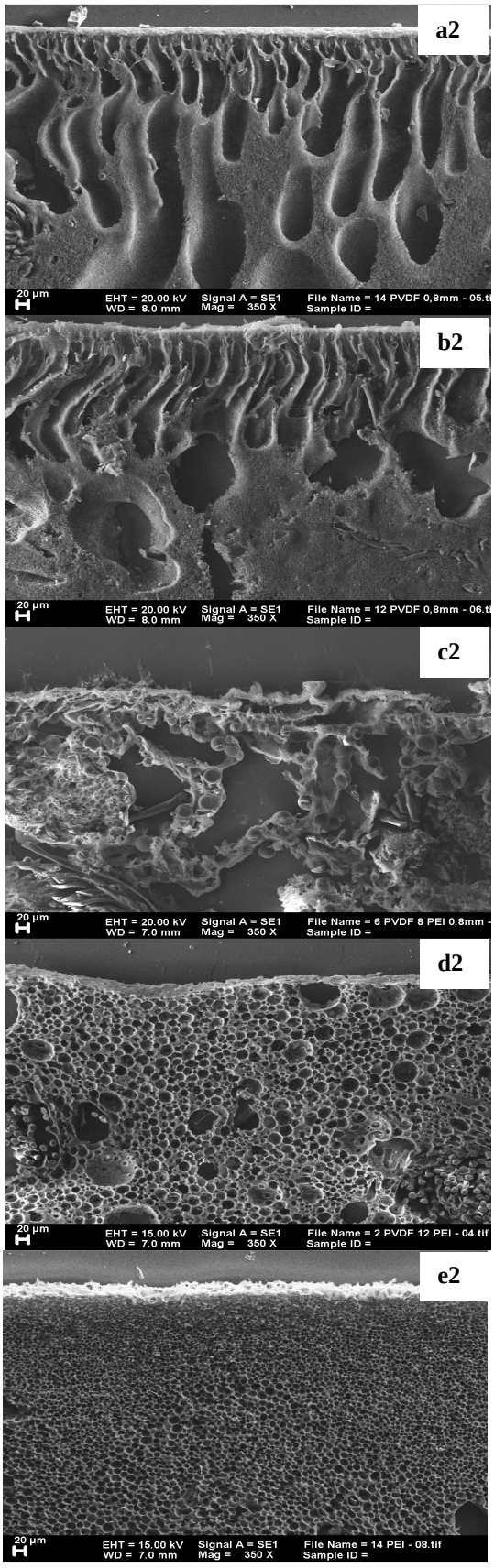

Fig. 2 SEM images of the cross-section morphologies of the M1 (a2), M2 (b2), M5 (c2), M7 (d2), and M8 (e2) membrane

This finding is slightly different from previous studies which produced asymmetric PEI membranes with lower pore sizes [35]. This condition is thought to occur due to differences in pyrogen additives. The molecular structure of PEG much larger than NH_4Cl triggers the emergence of larger micropores on the membrane.

TABLE II
POROSITY AND PORE SIZE OF MEMBRANE WITH DIFFERENT COMPOSITION OF CASTING SOLUTION

Membrane	Porosity (%)	Pore Size (nm)
M1	17.39	0.366
M2	18.04	0.289
M3	9.32	0.279
M4	7.32	0.204
M5	7.19	0.196
M6	11.60	0.430
M7	18.93	0.453
M8	19.77	0.515

Significant differences in porosity and pore size of pure PVDF and PEI, as well as PVDF/PEI composites membranes, indicate that PVDF and PEI polymers blending has resulted in the membrane structural changes, which refers to both characteristics. Fig. 2 shows that all PVDF/PEI composite membranes detected have an asymmetrical structure consisting of a denser skin layer and a porous layer that includes micropores and macro void. The appearance of a number of large pores, especially on membranes M7 and M8, does not necessarily produce low porosity and large pore size in both. The degree of pore size distribution is the only explanation that allows the formation of asymmetry membranes with high porosity and pore size at the same time on PEI membranes and PEI-dominated composite membranes. In addition to influencing membrane structure, the homogeneity of the PVDF and PEI mixture (see SEM-EDX in Fig. 3) generally also influences mechanical characteristics and performance, as well as thermal and chemical resistance of membranes. Discussion of this matter is discussed later.

SEM-EDX analysis shows that the dominance of the presence of positively charged (C) and negatively charged (O and N) atoms in the molecular structure of PEI has resulted in membranes with higher porosity compared to PVDF. This finding is in line with the results of membrane cross-section morphology in Fig. 2 as well as porosity analysis results in Table II. According to this, the appearance of finite large pores, especially on the M8 membrane is predicted to be closely related to the width of the pore size distribution on the membrane as a result of an imperfect dissolution process, as seen in the results of SEM-EDX of M7 and M8 membranes (Fig. 3(d3) and (e3)). In Fig. 3(d3) it appears that the N and O atoms typical of PEI polymers were not evenly distributed in the analyzed membrane. The same thing is also seen in the results of SEM-EDX membrane 8 (Fig. 3(e3)). Furthermore, detection of fluorine (F) atoms contamination on the M8 membrane also influences membrane formation with characteristics slightly different from previous studies [35]. However, it is important to further analyses the pore size distribution on the membranes of M1, M2, M5, M7 and M8 to strengthen the assumption.

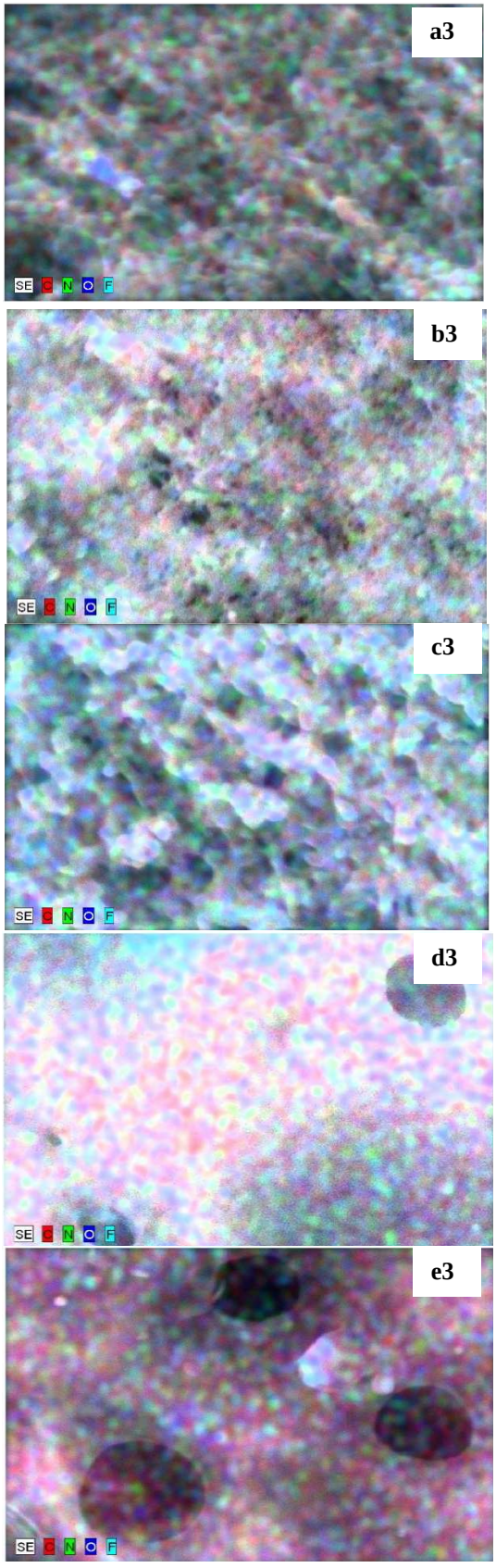

Fig. 3 SEM-EDX images of the M1 (a3), M2 (b3), M5 (c3), M7 (d3), and M8 (e3) membrane

TABLE III
ATOM DISTRIBUTION ON MEMBRANE WITH DIFFERENT COMPOSITION OF CASTING SOLUTION

	Atom. C (at.%)			
Membrane	**F**	**C**	**O**	**N**
M1	46.36	53.50	0.11	0.02
M2	48.35	50.97	0.66	0.02
M5	41.53	57.85	0.54	0.08
M7	5.69	71.45	20.02	2.84
M8	2.45	71.09	21.11	5.36

B. Chemical Characterization of the Membrane

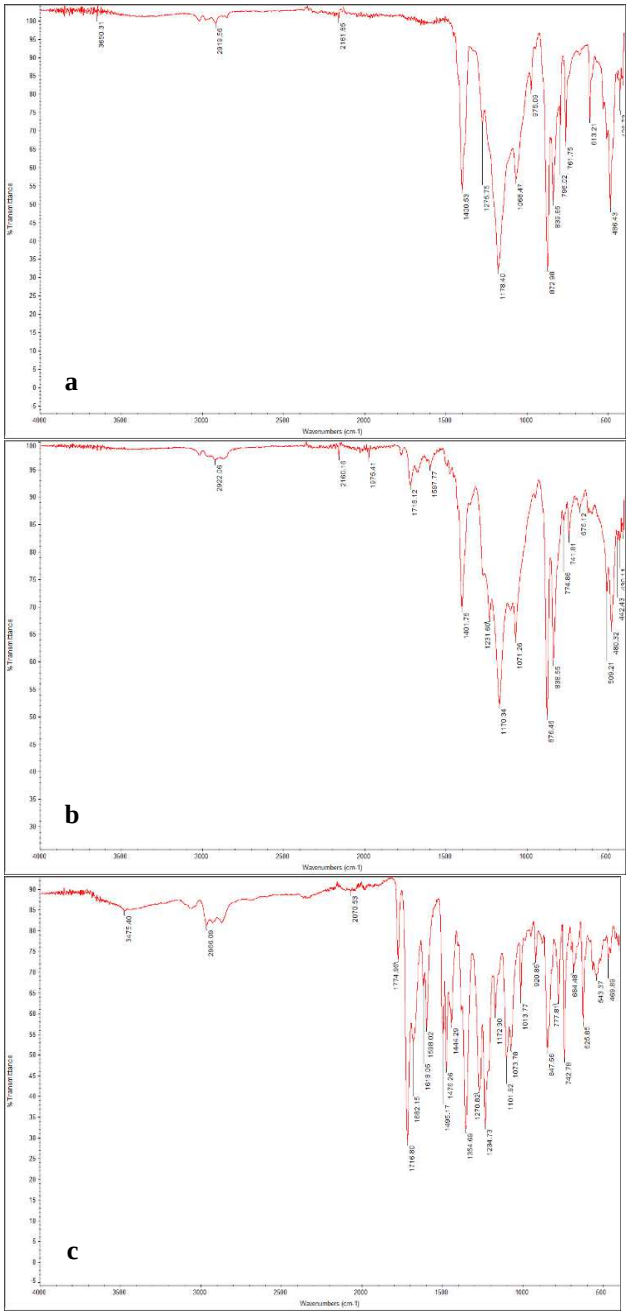

Fig. 4 Infrared membrane spectra: M1 (a); M4 (b) and M8 (c)

FTIR analysis can confirm the successful formation of PVDF/PEI composite membranes. The infra-red spectra of the pure PVDF and PEI membrane were used as a comparison and on Fig. 4, showing the infra-red spectra of pure PVDF (M1) (a), PVDF/PEI composite (M4) (b), and pure PEI (M8) membrane (c). The formation of the PVDF/PEI composite membrane has been successfully confirmed. In the infra-red spectra of the M4 membrane has detected the appearance of a new peak at wave number 1400-1600 cm^{-1} given by the conjugated and aromatic C=C functional groups when compared to the M1. It also detected a new peak appearance at 970-1250 cm^{-1} (1000-1300 cm^{-1}); 1000-1250 cm^{-1}; and 1710-1720 cm^{-1} each attributed to the presence of C-O (C-O ether), C-N and C=O functional groups. This condition confirms the presence of PEI in the M4 membrane. Meanwhile, the appearance of a new peak in the wavenumbers 1000-1400 cm^{-1} in the infra-red spectra of the M4 membrane when compared with the M8 membrane has further strengthened the formation of the PVDF/PEI composite membrane through detection of the C-F typical peak belonging to the PVDF molecular structure. In Fig. 5 (a and b) the molecular structure of PVDF and PEI is apparent.

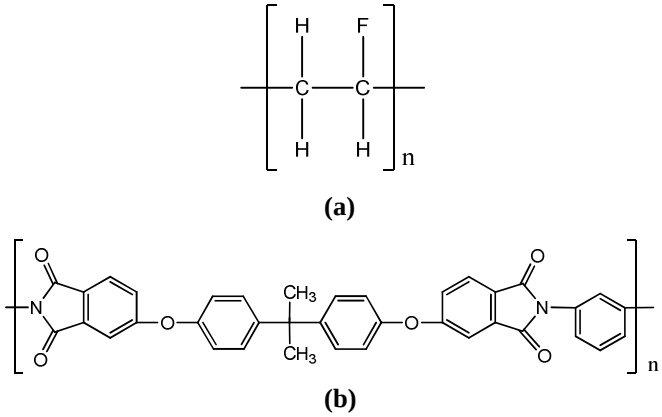

Fig. 5 Molecular structure of PVDF (a); and PEI (b)

C. Mechanical Characterization of the Membrane

Mechanical strength of pure PVDF; PVDF/PEI composite and pure PEI membrane using the non-woven support are shown in Fig. 6. The results show a decrease in Young's modulus values of the PEI membrane and an increase of the PVDF membrane, each along with the increasing levels of PVDF and PEI added to the casting solution. This condition is induced by the tendency of charge differences generated by various functional groups in PEI molecular structures which are much more complex and larger than PVDF, which further results in a greater bond strength on the PEI membrane compared with PVDF. The bond strength has resulted in a larger membrane strength (M7 and M8) in maintaining a specific pore size when obtaining external loads. This fact further strengthens the notion of the wide pore distribution of M7 and M8 membranes that are the background of the appearance of several large pores on the M7 and M8 membranes. The high value of Young's modulus of M7 and M8 membranes compared to M1 and M2 membranes show the formation of a typical PEI membrane structure that is rich in small pores. Unlike the general membrane, PEI's typical pore structure generally not trigger low permeability, as to be discussed next.

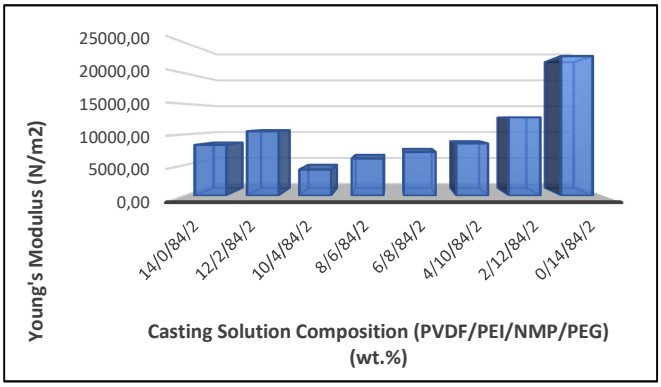

Fig. 6 Mechanical strength of the membrane with a different casting solution composition

D. Flux Test and Filtration Experiment

Pure water flux (PWF) of pure PVDF, PVDF/PEI composite and pure PEI membrane with different casting solution composition were evaluated at operational pressure of 1 bar, and the results had shown in Fig. 7. The results showed that the PWF of the pure PVDF membrane was equal to 3674.67 $Lm^{-2}h^{-1}bar^{-1}$, whereas the pure PEI membrane showed PWF of 7349.34 $Lm^{-2}h^{-1}bar^{-1}$. Whereas in composite membranes (M2 and M5), PWF is detected lower than PVDF membranes. However, a further increase in PEI levels in the cast solution (M7 and M8) has resulted in membranes with higher porosity, thus inducing higher PWF gains. Initially, the slight addition of the PEI to the casting solution has increased the membrane pore density. However, an increase in PEI levels that are more extreme in the casting solution has produced membranes with porosity and pore size typical of PEI.

In general, the permeability of porous membranes is strongly influenced by the membrane porosity, pore size and hydrophilic properties to a certain extent. Based on SEM, porosity and pore size analysis results can be predicted that high permeability of PEI membrane was more related to high porosity properties compared to the pore size of the membrane. This condition is triggered by a much higher porosity of the PEI membrane than PVDF. The high porosity of the PEI membrane has offset the presence of small pore sizes that are predicted to be abundant in the membrane. Thus, in general, PVDF blending with PEI polymer has created an asymmetrical structure with smaller pore sizes, but with much higher porosity. This characteristic results in a higher PWF value on the PEI membrane.

In contrast to PWF which is generally affected solely by membrane porosity, pore size and hydrophilic properties, the separation of feed solutions with specific solutes are also strongly influenced by the size and shape of solute particles in the feed solution. The flux produced by the pure PVDF (M1), the PVDF/PEI composite (M4) and the pure PEI membrane (M8) have shown in Fig. 8. It can be seen that the resulting flux from separation $CaCl_2$, $CuSO_4$ and $MgCl_2$ each becomes the highest for M1 (1201.78 $Lm^{-2}h^{-1}bar^{-1}$), M4 (1292.85 $Lm^{-2}h^{-1}bar^{-1}$), and M8 (1325.12 $Lm^{-2}h^{-1}bar^{-1}$) and vice versa on separation $CuSO_4$ for M1(347.42 $Lm^{-2}h^{-1}bar^{-1}$) as well as sucrose each for M4 (500.48 $Lm^{-2}h^{-1}bar^{-1}$) and M8 (370.89 $Lm^{-2}h^{-1}bar^{-1}$), produced the lowest flux on the three membranes tested. This condition is closely related to the suitability of the pore sizes of the three membranes with the size of dissolved metal salts and sucrose particles. In addition, the electronegativity of each metal element has a more significant effect on the degree of separation or flux. Related to this, the tendency of negative charges on the membrane becomes a significant obstacle to the rate of separation of the feed solution with higher electronegativity. These two parameters are one of the causes of the lower/higher flux of each membrane.

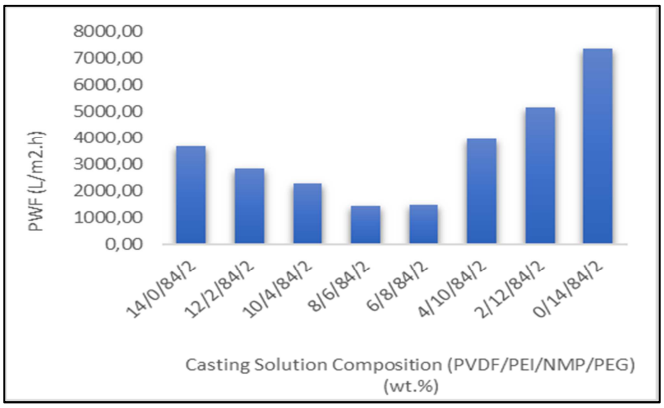

Fig. 7 Pure water flux of the membrane with a different casting solution composition

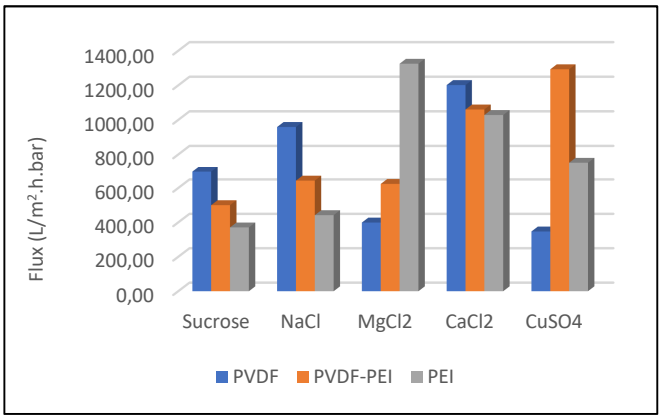

Fig. 8 The flux of the membrane: (a) M1; (b) M4; and (c) M8 for the separation of soluble metal salts and sucrose

The porosity of the PEI membrane that is far above the other two membranes has produced a higher flux on the PEI membrane, but the small pore size predicted to be abundant in the membrane has been one of the causes of differences in permeability of dissolved metal salts and sucrose. A pore size that is too small triggers an increase in the potential for impurities and causes a decrease in flux to a certain point due to blockage rather than narrowing in the membrane pores.

E. Thermal Resistance

To evaluate the thermal resistance, TGA measurements of pure PVDF (M1), PVDF/PEI composite (M4) and pure PEI membrane (M8) were obtained. The results show higher thermal stability due to an increase in the addition of PEI to the casting solution. The thermogravimetric analysis is showing PVDF decomposition in several steps at the lower temperature shown in Fig. 9(a). Decomposition was detected from the weight lost during the tested temperature range. The first mass reduction detected in the 165-170 °C is

predicted to be closely related to the water molecules release from within the membrane matrix as a vapor. The second phase mass reduction, occurring at a temperature range of 170-345 °C, is predicted to be the time when evaporation of an adsorbed NMP solvent has occurred on the membrane. The third phase mass reduction was found to occur in the 345- 555 °C. This third-stage mass reduction is predicted to be closely related to PVDF decomposition. The results are in line with those published in [7] which report the occurrence of PVDF decomposition at temperatures around 375 °C. To ascertain the cause of each mass reduction step, a functional group analysis of the M1 membrane using FTIR was performed. The infrared spectra of the membrane from each of the mass reduction steps are presented in Fig. 10.

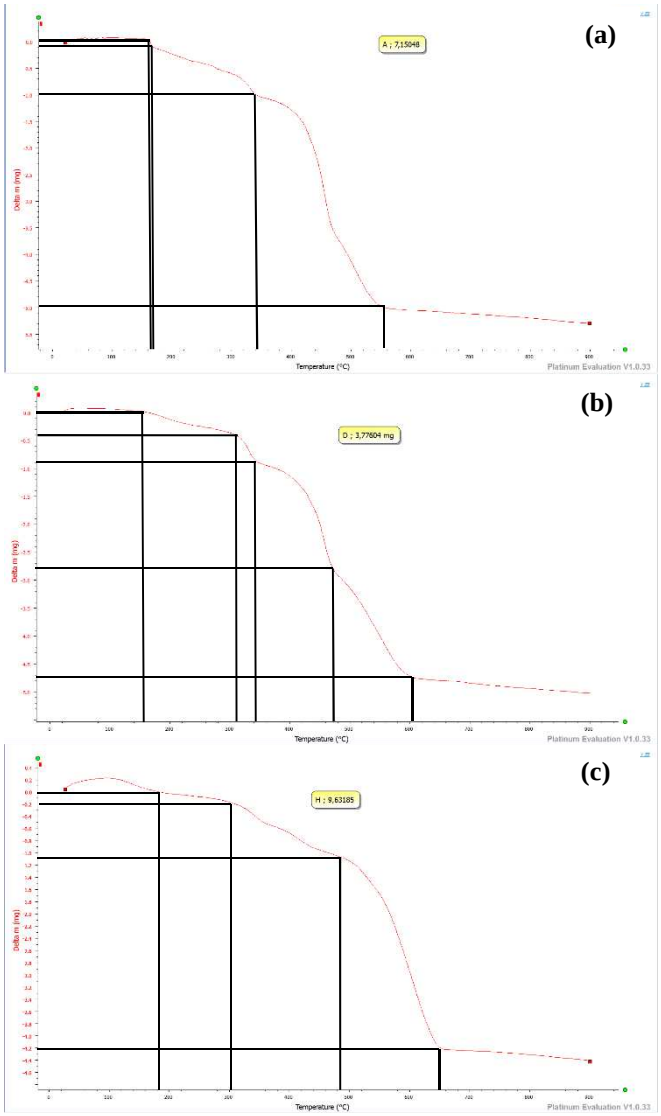

Fig. 9 Thermogram of the membrane: (a) M1; (b) M4; and (c) M8

The results of the analysis with increased thermal stability are shown by thermogram (Fig. 9(b)) of the PVDF/PEI composite membrane (M4). Increased thermal stability is detected from the occurrence of decomposition with the same stages in the higher heating temperature. The first mass reduction showing the loss of water molecules from the M4 membrane was detected at a higher temperature range compared to the M1 membrane, i.e., at 158-310 °C. The occurrence of increased membrane matrix density formed as a result of PVDF-PEI polymer blending has inhibited the occurrence of water molecules from within the membrane matrix. This condition has triggered a higher heat required to be able to evaporate all water molecules from the membrane matrix. The same conditions were detected in the next, second and third mass reduction stages. The second phase mass reduction of the M4 membrane occurs in the temperature range 310-345 °C. The increased pore density of the M4 membrane matrix is also predicted to inhibit the occurrence of unwashed and depleted NMP evaporation from the membrane matrix. Thus, higher heat energy is required to be able to evaporate NMP from the membrane matrix. Meanwhile, the decomposition of PVDF detected at the third stage mass reduction took place at a temperature range not significantly different from that of the M1 membrane, i.e. at 345-475 °C. In addition, in the TGA test of the M4 membrane, it has detected a fourth phase mass reduction in the temperature range 475-605 °C. This fourth-stage mass reduction is predicted to be due to the decomposition of PEI molecules from the M4 membrane matrix. This finding is in line with [34], which reports PEI decomposition at temperatures around 500 ˚C. This finding is also reinforced by FTIR analysis. The M4 membrane IR spectra from each mass reduction stage are shown in Fig. 11.

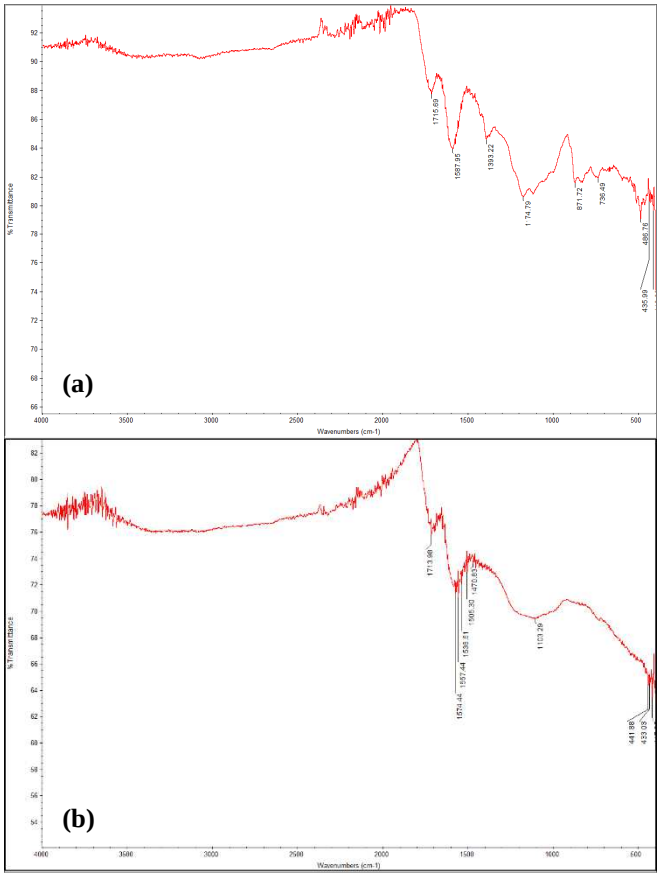

Fig. 10 FT-IR spectra of the M1 membrane at: (a) 375 °C (PVDF degradation temperature); and (b) 500 °C (PEI degradation temperature)

It is associated with the thermal stability of the M8 membrane, the thermogram in Fig. 9(c) shows the highest thermal stability compared to the two other membranes (M1 and M4). The first and second detectable phase mass

reductions of the M8 membrane show much higher temperatures required to be able to remove H_2O and NMP molecules from within a pure PEI membrane matrix that predicted has many small pore sizes. To be able to release the H_2O molecules contained in the M8 membrane matrix, it is required to heat to a temperature range of 180-305 °C, while to remove the remaining and deposited NMP solvent in the M8 membrane matrix, heating is required in the 305-485 °C temperature range. The third phase mass reduction in the M8 membrane occurs in the temperature range 485-655 °C. This result is in accordance with the result of the FTIR analysis. The M8 membrane IR spectra from each mass reduction stage are shown in Fig. 12.

The M1 membrane infra-red spectra which have been tested for thermal resistance at the degradation temperature of PVDF (375 ° C) in Fig. 10 (a) shows the appearance of several typical PVDF functional groups, including C=C at 1587.95 cm^{-1} and -CF at 1393.22 cm^{-1} and 1174.79 cm^{-1}. Furthermore, more C=C functional groups have been found, namely at 1574.44 cm^{-1}; 1557.44 cm^{-1}; 1538,61 cm^{-1}; 1505.30 cm^{-1}; and 1470.83 cm^{-1}. While the functional group -CF only detected its appearance at 1103.29 cm^{-1}. The increase in C=C along with the reduction of -CF functional groups in the IR spectra of PVDF membranes (Fig. 10(b)) becomes a marker of the *dehydrofluorination*, namely the loss of -HF functional groups which generally trigger the formation of C=C functional groups in the PVDF molecular structure.

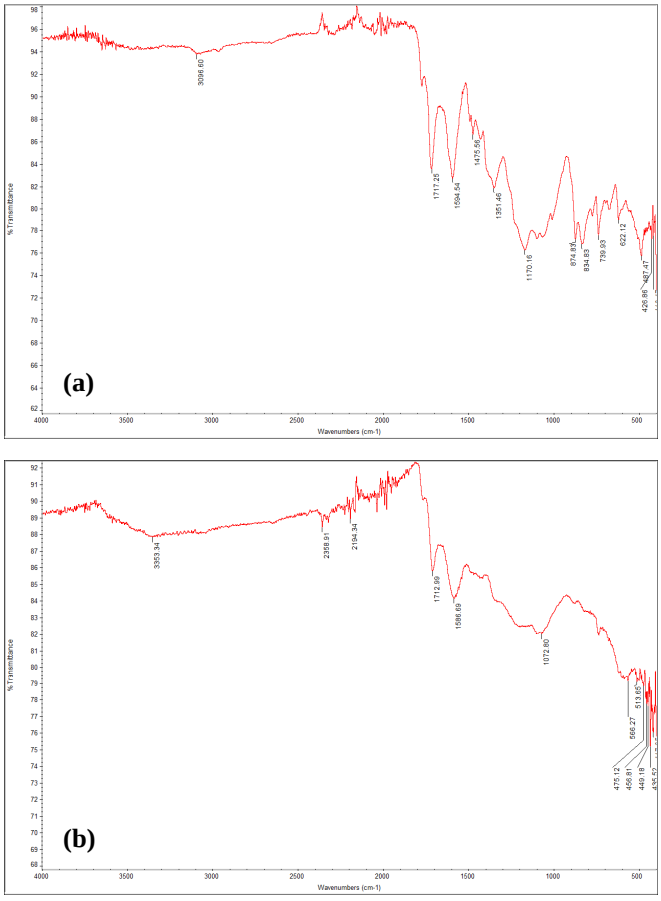

Fig. 11 FT-IR spectra of the M4 membrane at : (a) 375 °C (PVDF degradation temperature); and (b) 500 °C (PEI degradation temperature)

The FTIR results of the M4 membrane that have passed the thermal resistance test at 375 °C and 500 °C are shown in Fig. 11. The results show the appearance of =C-H & $=CH_2$ functional groups at 3095.60 cm^{-1}; C=O at 1717.25 cm^{-1}; C=C at 1594.54 cm^{-1}, and 1475.56 cm^{-1}; C-F at 1351.46 cm^{-1} and 1170.16 cm^{-1}; C-H/NH_2 & NH at 874.83 cm^{-1}, 834.83 cm^{-1}, and 739.93 cm^{-1}; and C-H deformation at 622.12 cm^{-1}. While the thermal resistance test at a temperature of 500 °C only leaves the appearance of the N-H (2° amine) functional group at 3353.34 cm^{-1}; C=O at 1712.99 cm^{-1}; C=C at 1586.69 cm^{-1}; and C-F at 1072.80 cm^{-1}. These results indicate the existence of PEI characteristic functional groups that are more dominant in M4 composite membranes compared to PVDF after heating at 500 °C.

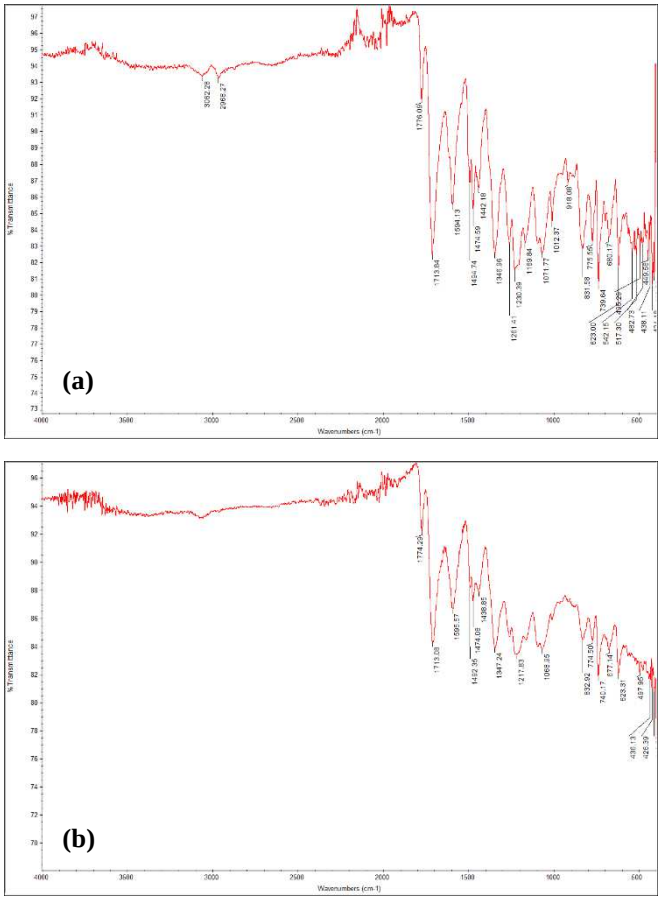

Fig. 12 FT-IR spectra of the M8 membrane at: (a) 375 °C (PVDF degradation temperature); and (b) 500 °C (PEI degradation temperature)

The FTIR results of the M8 membrane (Fig. 12) show the high thermal resistance of PEI membranes compared to PVDF/PEI and PVDF membrane. This can be seen from the existence of a large number of PEI typical functional groups, such as =C-H and $=CH_2$ at 3062.28 cm^{-1}; CH_3, CH_2 and CH at 2968.27 cm^{-1}; C=O at 1776.09 cm^{-1}, 1713.84 cm^{-1}, 1594.13 cm^{-1}, 1494.74 cm^{-1}, 1474.59 cm^{-1}, and 1442.18 cm^{-1}; C-O ether at 1346.96 cm^{-1} and 1261.41 cm^{-1}; C-O ether which overlapped with C-N at 1230.39 cm^{-1}, 1169.84 cm^{-1}, 1071.77 cm^{-1}, and 1012, 37 cm^{-1}; C-H which overlapped NH at 918.08 cm^{-1}, 831.58 cm^{-1}, 775.55 cm^{-1}, and 739.64 cm^{-1}; and C-H deformation at 680.17 cm^{-1}. In general, the IR spectra of the M8 membrane that have been heated at 500 °C

did not show significant differences, which still detected the appearance of a large number of PEI typical functional groups such as C=O, C=C, C-O ether, CN, CH, NH_2 and NH as well as CH deformation. These findings strengthen the fact that the PEI membrane's thermal resistance is higher than that of PVDF/PEI composite and PVDF membranes.

F. Chemical Resistance

Fig. 13 shows the FTIR results of the pure PEI membrane, before and after immersing in sulfuric acid 80 vol.%. The results show the appearance of peaks in a number of specific wavenumbers. Before going through chemical resistance tests in an acidic environment, the IR spectra of the PEI membrane showed the appearance of functional groups at 3475.40 cm^{-1} (N-H, 1° amine); 2966.09 cm^{-1} (CH_3, CH_2 and CH); 1774.96 cm^{-1}, 1716.80 cm^{-1}, 1682.15 cm^{-1} (C=O); 1618.05 cm^{-1} and 1598.02 cm^{-1} (NH_2 scissoring); 1495.17 cm^{-1}, 1476.26 cm^{-1} (C=C); 1444.29 cm^{-1} (C=C overlapped with CH_2 and CH_3 deformation); 1354.69 cm^{-1} (CH_2 and CH_3 deformation); 1234.73 cm^{-1} (C-O ether); 1234.73 cm^{-1}, 1172.30 cm^{-1}, 1101.92 cm^{-1}, 1073.78 cm^{-1}, and 1013.77 cm^{-1} (C-O ether overlapped with C-N); 920.85 cm^{-1}, 847.56 cm^{-1}, 777.81 cm^{-1}, 742.78 cm^{-1}, and 742.78 cm^{-1} (C-H overlapped with NH_2 and NH); and 684.48 cm^{-1} (C-H deformation). However, several peaks were detected disappearing from the IR spectra of the PEI membrane, which were treated in sulfuric acid. This indicates the loss of several functional groups, such as C=O at 1682.15 cm^{-1} and C-H, which overlapped with NH_2 and NH at 920.85 cm^{-1}. The loss of some functional groups is a marker of PEI membrane resistance that is not very good in an environment of sulfuric acid 80 vol.%.

In addition, the results also showed lower stability of PEI in the sulfuric acid environment than PVDF. This is evident from the decrease in intensity or even to the loss of PEI peak characteristics in the infra-red spectrum of the PVDF/PEI membrane that has been immersed in 80vol.% sulfuric acid for 24 hours. The peak characteristics are those that occur at 2922.06 cm^{-1} (CH_3, CH_2 and CH); 2160.16 cm^{-1} (-N=C=O/C=C=O); 1975.41 cm^{-1} (C=C asymmetry stretching); 1597.77 cm^{-1} (NH_2 scissoring); 1231.60 cm^{-1} (C-O ether overlapped with C-N and C-F). These results are in line with findings [7] that report the good chemical stability of PVDF polymers in sulfuric acid environments. This condition is clearly seen in the IR spectrum of the PVDF/PEI membrane in Fig. 14.

The FTIR analysis results of the M1 membrane, before and after immersing in sulfuric acid 80 vol.% (Fig. 15) further strengthens the fact that the chemical resistance of PVDF membranes is higher than PEI in acidic environments. In M1 membrane (before immersion) is detected the appearance of peaks at 2919.56 cm^{-1} (CH_3, CH_2 and CH); 1400.53 cm^{-1} (C=C overlap with CH_2 and CH_3 deformation); 1178.40 cm^{-1} and 1068.47 cm^{-1} (C-F); 872.98 cm^{-1}, 839.65 cm^{-1}, and 761.73 cm^{-1} (C-H); and at 613.21 cm^{-1} (C-H deformation). The appearance of the peaks was also detected in the results of IR analysis (after immersion). This shows the high chemical stability of PVDF membranes in an acidic environment.

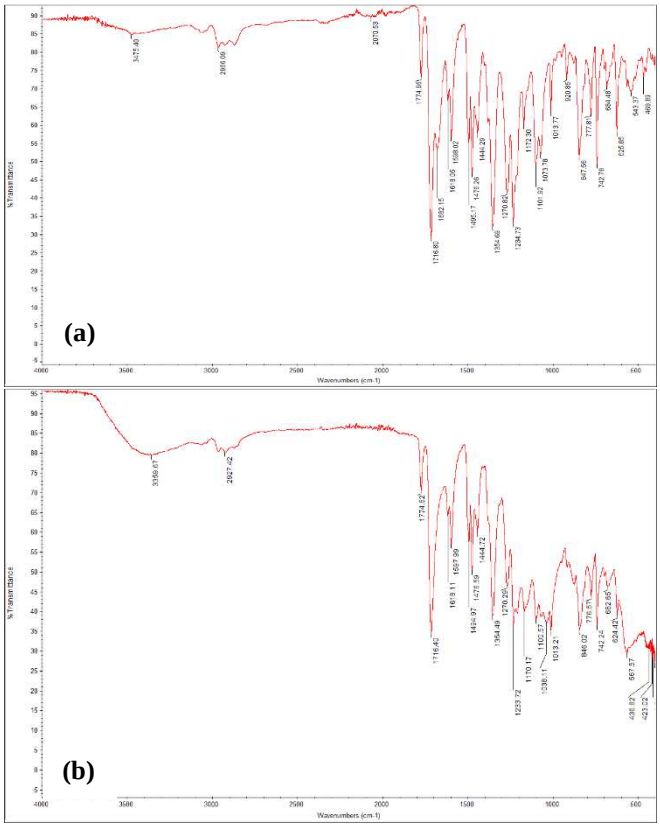

Fig. 13 FT-IR spectra of the M8 membrane: before (a) and after (b) immersion in 80vol.% sulfuric acid

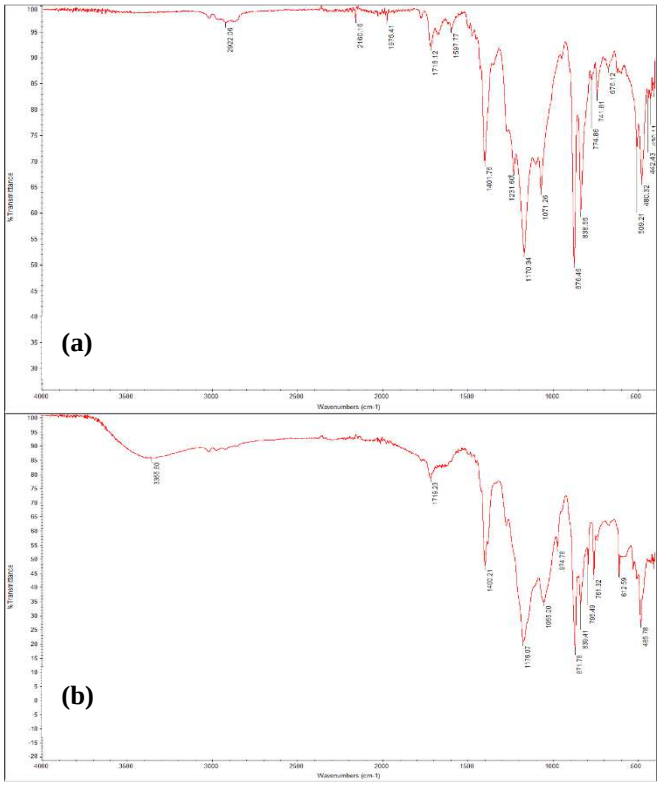

Fig. 14 FT-IR spectra of the M4 membrane: before (a) and after (b) immersion in 80vol.% sulfuric acid

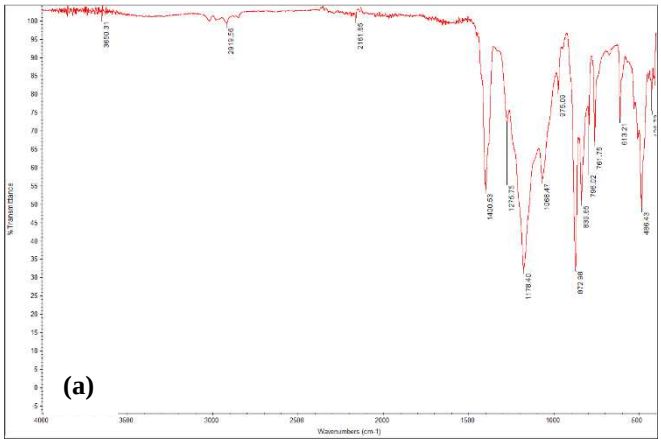

Fig. 15 FT-IR spectra of the M1 membrane: before (a) and after (b) immersion in 80vol.% sulfuric acid

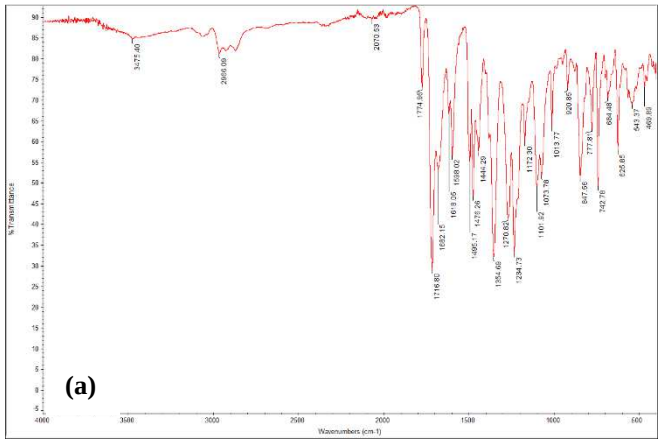

Fig. 16 FT-IR spectra of the M8 membrane: before (a) and after (b) immersion in 80wt.% sodium hydroxide

The result of chemical stability test of PVDF/PEI membrane in alkaline environment showed low chemical resistance of PVDF in the alkaline environment. However, alkaline resistance of PVDF membranes is still higher when compared to PEI membranes. Based on IR spectra of the PEI membrane (M8), before and after treatment in alkaline environments, has been detected the losses of N-H (1° amine) functional group at 3475.40 cm^{-1}; C=O at 1774.96 cm^{-1}, 1716.80 cm^{-1} and 1682.15 cm^{-1}; NH_2 scissoring at 1618.05 cm^{-1} and 1598.02 cm^{-1}; C=C at 1495.17 cm^{-1} and 1476.26 cm^{-1}; C-O ether at 1270.82 cm^{-1}; C-O ether was overlapped with C-N at 1234.73 cm^{-1}, 1172.30 cm^{-1}, 1101.92 cm^{-1} and 1013.77 cm^{-1}; C-H which overlapped with NH_2 and NH at 920.85 cm^{-1}, 777.81 cm^{-1} and 742.78 cm^{-1}.

This finding was also strengthened by the FTIR results of the M4 composite membrane, where a large number of PEI typical functional groups losses were also detected, namely at 1718.12 cm^{-1} (C=O); 1597.77 cm^{-1} (NH_2 scissoring); 1231.60 cm^{-1} and 1170.34 cm^{-1} (C-O ether); and at 774.86 cm^{-1} and 741.81 cm^{-1} (C-H which overlapped with NH_2 and NH). A detailed description of the changes that occur in the M4 membrane functional group after treatment in an alkaline environment is presented in Fig. 17.

The physical changes in membrane PVDF (M1) which gradually turns brown and eventually turns into the black after immersion in 80 wt.% *sodium hydroxides* indicate a significant change in the functional groups of the membrane. Based on the IR spectra of the M1 membrane before and after treatment in an alkaline environment it was detected the loss of a number of peaks at specific wavenumbers, including 798.02 cm^{-1} and 839.65 cm^{-1} indicating the loss of the C-H bending functional group, 975 cm^{-1} indicating a =C-H and $=CH_2$ functional group loss, and at 1275.75 cm^{-1} which indicates the loss of the C-F functional group.

The results of this analysis are closely related to dehydrochlorination, i.e. the loss of the H-F functional group of PVDF structures. This finding is consistent with the publication of a number of researchers who claimed the same color change after treatment for several hours [7], [23], [34], [36], [37]. The PVDF dehydrochlorination has triggered the appearance of a typical peak of the C=C functional group in pure PVDF membrane spectra, as shown in Fig. 18.

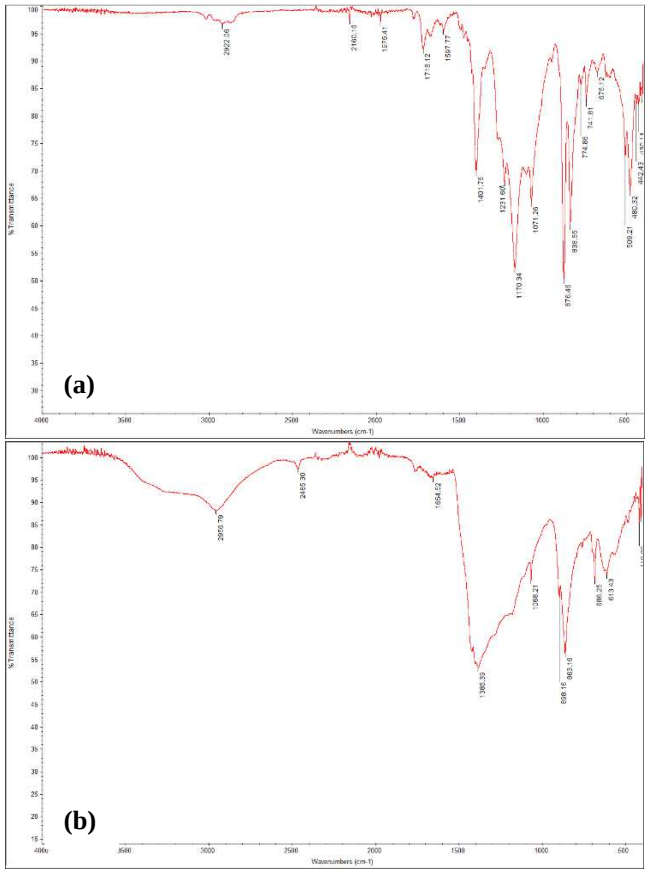

Fig. 17 FT-IR spectra of the M4 membrane: before (a) and after (b) immersion in 80wt.% sodium hydroxide

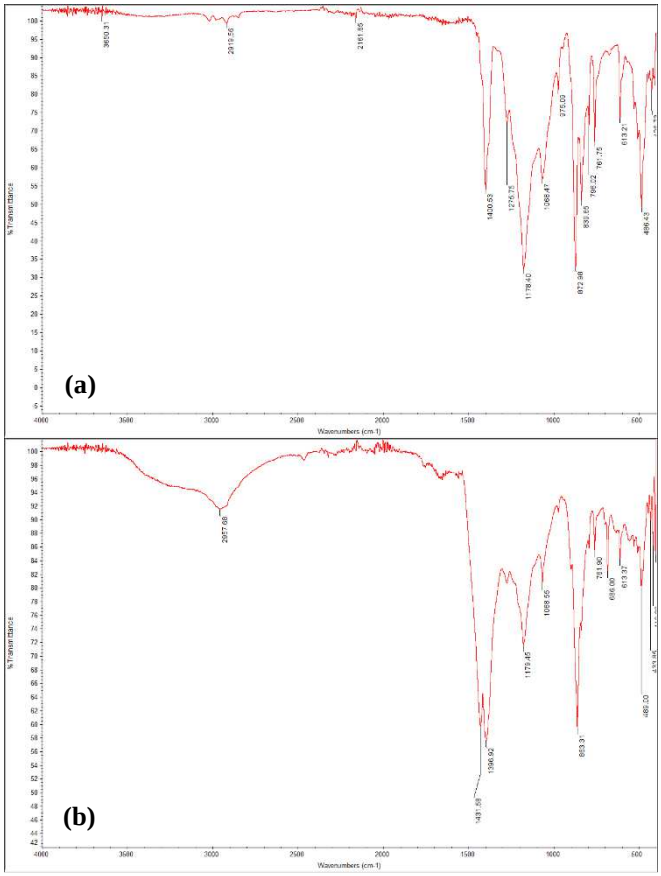

Fig. 18 FT-IR spectra of the M1 membrane: before (a) and after (b) immersion in 80wt.% sodium hydroxide

IV. Conclusion

PVDF/PEI composite membrane with different PEI levels have been prepared by non-solvent induced phase separation method involving PEG-6000 as pore-forming additive. The effect of increasing PEI levels in casting solution against membrane characteristics and performance has been investigated. The results obtained can be summarized as follows. All PVDF/PEI composite membranes are found to have asymmetric pore structure (a combination of finger-like and sponge-like pores). An increase in PEI content of up to 8% (wt.%) in the PVDF matrix has reduced porosity and pore size, especially in porous layers of PVDF/PEI composite membranes. Meanwhile elevated PEI levels in the range 10 (wt%)-14 (wt.%) actually increases membrane porosity and pore size. An increase in PEI content of up to 8% in the PVDF matrix has reduced porosity as well as micropore and macro void size in PVDF/PEI composite membrane porous layers. The addition of PEI levels in the casting solution has increased the ratio of stress to the membrane strain. Increasing levels of PEI in the range of 2 (wt%)-8 (wt.%) in the casting solution has decreased PWF, while increasing levels of PEI in the range 10 (wt%)-14 (wt.%) have the opposite effect, increased PWF on the membrane. Increased levels of PEI in a casting solution have varied effects on the permeability of dissolved metal salts and sucrose. PVDF/PEI composite membrane has a higher resistance to acid than pure PEI membrane and lower than pure PVDF membrane. PVDF/PEI composite membrane has lower resistance to the base than pure PEI membrane and higher than pure PVDF membrane.

Acknowledgement

The researcher would like to thank the Ministry of Research and Technology - Higher Education of Indonesia (KEMENRISTEK/BRIN) for the financial support provided through the College Superior Research Program given in the fiscal year 2018 and to the department of chemistry, faculty of mathematics and science, Universitas Negeri Surabaya for infrastructure support to this study.

References

[1] M. S. Diallo, N. A. Frommer, and M. S. Jhon, "Nanotechnology for sustainable development: Retrospective and outlook," *Journal of Nanoparticle Research*, vol. 15, no. 11. 2013, doi: 10.1007/s11051-013-2044-0.

[2] M. Rao Kotte, T. Hwang, J. I. Han, and M. S. Diallo, "A one-pot method for the preparation of mixed matrix polyvinylidene fluoride membranes with in situ synthesised and PEGylated polyethyleneimine particles," *J. Memb. Sci.*, vol. 474, pp. 277–287, 2015, doi: 10.1016/j.memsci.2014.09.044.

[3] S. Gouda, R. G. Kerry, G. Das, S. Paramithiotis, H. S. Shin, and J. K. Patra, "Revitalisation of plant growth-promoting rhizobacteria for sustainable development in agriculture," *Microbiological Research*, vol. 206. pp. 131–140, 2018, doi: 10.1016/j.micres.2017.08.016.

[4] C. M. Papapostolou, E. M. Kondili, D. P. Zafirakis, and G. T. Tzanes, "Sustainable water supply systems for the islands: The integration with the energy problem," *Renew. Energy*, vol. 146, pp. 2577–2588, 2020, doi: 10.1016/j.renene.2019.07.130.

[5] M. M. Wagh and V. V. Kulkarni, "Thermal energy demand fulfilment of Kolhapur through modelling and optimisation of integrated renewable energy systems," *Renew. Energy Focus*, vol. 29, pp. 114–122, 2019, doi: 10.1016/j.ref.2019.03.004.

[6] X. Wang, Z. Wang, Z. Wang, Y. Cao, and J. Meng, "Tethering of hyperbranched polyols using PEI as a building block to synthesise

antifouling PVDF membranes," *Appl. Surf. Sci.*, vol. 419, pp. 546–556, 2017, doi: 10.1016/j.apsusc.2017.05.037.

[7] N. Kusumawati, P. Setiarso, M. M. Sianita, and S. Muslim, "Transport properties, mechanical behaviour, thermal and chemical resistance of asymmetric flat sheet membrane prepared from PSf/PVDF blended membrane on gauze supporting layer," *Indones. J. Chem.*, vol. 18, no. 2, pp. 257–264, 2018, doi: 10.22146/ijc.27272.

[8] C. Z. Liang, T. S. Chung, and J. Y. Lai, "A review of polymeric composite membranes for gas separation and energy production," *Progress in Polymer Science*, vol. 97. 2019, doi: 10.1016/j.progpolymsci.2019.06.001.

[9] E. Lasseuguette and M. C. Ferrari, "Polymer membranes for sustainable gas separation," in *Sustainable Nanoscale Engineering: From Materials Design to Chemical Processing*, 2019, pp. 265–296.

[10] N. Kusumawati, P. Setiarso, S. Muslim, and N. Purwidiani, "Synergistic ability of PSf and pvdf to develop high-performance PSf/PVDF coated membrane for water treatment," *Rasayan J. Chem.*, vol. 11, no. 1, pp. 260–279, 2018, doi: 10.7324/RJC.2018.1112018.

[11] N. Kusumawati, P. Setiarso, and S. Muslim, "Polysulfone/polyvinylidene fluoride composite membrane: Effect of coating dope composition on membrane characteristics and performance," *Rasayan J. Chem.*, vol. 11, no. 3, pp. 1034–1041, 2018, doi: 10.31788/RJC.2018.1133020.

[12] E. Elele *et al.*, "Mechanical properties of polymeric microfiltration membranes," *J. Memb. Sci.*, vol. 591, 2019, doi: 10.1016/j.memsci.2019.117351.

[13] K. H. Oh, Y. H. Ko, and K. J. Kim, "Mechanical properties of amorphous PEI, PES, and PVC up to 11 GPa studied by Brillouin light scattering," *Phys. B Condens. Matter*, vol. 576, 2020, doi: 10.1016/j.physb.2019.411722.

[14] U. Sathya, M. Nithya, and Keerthi, "Fabrication and characterisation of fine-tuned Polyetherimide (PEI)/WO3 composite ultrafiltration membranes for antifouling studies," *Chem. Phys. Lett.*, vol. 744, 2020, doi: 10.1016/j.cplett.2020.137201.

[15] Y. Zhu, W. Xie, J. Li, T. Xing, and J. Jin, "PH-Induced non-fouling membrane for effective separation of oil-in-water emulsion," *J. Memb. Sci.*, vol. 477, pp. 131–138, 2015, doi: 10.1016/j.memsci.2014.12.026.

[16] M. Vásquez-Rendón and M. L. Álvarez-Láinez, "Tailoring the mechanical, thermal, and flammability properties of high-performance PEI/PBT blends exhibiting dual-phase continuity," *Polymer (Guildf).*, vol. 154, pp. 241–252, 2018, doi: 10.1016/j.polymer.2018.09.012.

[17] H. Saleem, L. Trabzon, A. Kilic, and S. J. Zaidi, "Recent advances in nanofibrous membranes: Production and applications in water treatment and desalination," *Desalination*, vol. 478. 2020, doi: 10.1016/j.desal.2019.114178.

[18] A. Nasir, F. Masood, T. Yasin, and A. Hameed, "Progress in polymeric nanocomposite membranes for wastewater treatment: Preparation, properties and applications," *Journal of Industrial and Engineering Chemistry*, vol. 79. pp. 29–40, 2019, doi: 10.1016/j.jiec.2019.06.052.

[19] D. S. Dlamini, J. Li, and B. B. Mamba, "Critical review of montmorillonite/polymer mixed-matrix filtration membranes: Possibilities and challenges," *Applied Clay Science*, vol. 168. pp. 21–30, 2019, doi: 10.1016/j.clay.2018.10.016.

[20] T. H. Bae, J. S. Lee, W. Qiu, W. J. Koros, C. W. Jones, and S. Nair, "A high-performance gas-separation membrane containing submicrometer-sized metal-organic framework crystals," *Angew. Chemie - Int. Ed.*, vol. 49, no. 51, pp. 9863–9866, 2010, doi: 10.1002/anie.201006141.

[21] P. Van Rijn *et al.*, "Challenges and advances in the field of self-assembled membranes," *Chem. Soc. Rev.*, vol. 42, no. 16, pp. 6578–6592, 2013, doi: 10.1039/c3cs60125k.

[22] G. Dong, H. Li, and V. Chen, "Challenges and opportunities for mixed-matrix membranes for gas separation," *J. Mater. Chem. A*, vol. 1, no. 15, pp. 4610–4630, 2013, doi: 10.1039/c3ta00927k.

[23] R. D. C. Ningrum and N. Kusumawati, "Development and characterisation of polysulfone/polyvinylidene flouride blend membrane induced by delayed liquid-liquid demixing," *Int. J. Adv. Sci. Eng. Inf. Technol.*, vol. 6, no. 5, pp. 716–722, 2016, doi: 10.18517/ijaseit.6.5.911.

[24] N. Kusumawati, T. Koestiari, and S. Muslim, "The development of a new polymer membrane: PSF/PVDF blended membrane," *Res. J. Pharm. Biol. Chem. Sci.*, vol. 7, no. 4, pp. 69–77, 2016.

[25] N. Kusumawati, T. Koestiari, and M. Monica, "The influence of casting solution composition and stirring conditions against mechanical strenght and performance of polyvinylidene fluoride (PVDF)-polysulfone (PSf) composite membrane on textile industrial wastewater treatment," *Res. J. Pharm. Biol. Chem. Sci.*, vol. 6, no. 1, pp. 271–280, 2015.

[26] C. M. González-Henríquez, M. A. Sarabia-Vallejos, and J. Rodriguez-Hernandez, "Polymers for additive manufacturing and 4D-printing: Materials, methodologies, and biomedical applications," *Progress in Polymer Science*, vol. 94. pp. 57–116, 2019, doi: 10.1016/j.progpolymsci.2019.03.001.

[27] G. Bakeri, A. F. Ismail, T. Matsuura, M. S. Abdullah, B. C. Ng, and M. Mashkour, "Effect of PVDF blending on the structure and performance of PEI hollow fiber membrane in CO2 separation process," *Chem. Eng. Res. Des.*, vol. 104, pp. 367–375, 2015, doi: 10.1016/j.cherd.2015.08.024.

[28] L. Marbelia *et al.*, "Preparation of patterned flat-sheet membranes using a modified phase inversion process and advanced casting knife construction techniques," *J. Memb. Sci.*, vol. 597, 2020, doi: 10.1016/j.memsci.2019.117621.

[29] S. J. Lim and I. H. Shin, "Graft copolymerisation of GMA and EDMA on PVDF to hydrophilic surface modification by electron beam irradiation," *Nucl. Eng. Technol.*, vol. 52, no. 2, pp. 373–380, 2020, doi: 10.1016/j.net.2019.07.018.

[30] J. Zha *et al.*, "Superhydrophobicity of polymer films via fluorine atoms covalent attachment and surface nano-texturing," *J. Fluor. Chem.*, vol. 200, pp. 123–132, 2017, doi: 10.1016/j.jfluchem.2017.06.011.

[31] C. Sun and X. Feng, "Enhancing the performance of PVDF membranes by hydrophilic surface modification via amine treatment," *Sep. Purif. Technol.*, vol. 185, pp. 94–102, 2017, doi: 10.1016/j.seppur.2017.05.022.

[32] T. A. Agbaje, S. Al-Gharabli, M. O. Mavukkandy, J. Kujawa, and H. A. Arafat, "PVDF/magnetite blend membranes for enhanced flux and salt rejection in membrane distillation," *Desalination*, vol. 436, pp. 69–80, 2018, doi: 10.1016/j.desal.2018.02.012.

[33] Y. Ma, F. Shi, Z. Wang, M. Wu, J. Ma, and C. Gao, "Preparation and characterisation of PSf/clay nanocomposite membranes with PEG 400 as a pore forming additive," *Desalination*, vol. 286, pp. 131–137, 2012, doi: 10.1016/j.desal.2011.10.040.

[34] E. P. Setyaningsih, M. Machfudzoh, W. P. Utomo, and H. Fansuri, "Preparation of CaTiO3 asymmetric membranes using polyetherimide as binder polymer," *Indones. J. Chem.*, vol. 16, no. 1, pp. 20–24, 2016, doi: 10.22146/ijc.21172.

[35] N. Kusumawati, P. Setiarso, A. B. Santoso, S. C. Wibawa, and S. Muslim, "The development of pvdf/pei blended membrane: Effect of stirring time on membrane characteristics and performance," *Rasayan J. Chem.*, vol. 12, no. 2, pp. 975–986, 2019, doi: 10.31788/RJC.2019.1225104.

[36] F. Liu, N. A. Hashim, Y. Liu, M. R. M. Abed, and K. Li, "Progress in the production and modification of PVDF membranes," *Journal of Membrane Science*, vol. 375, no. 1–2. pp. 1–27, 2011, doi: 10.1016/j.memsci.2011.03.014.

[37] C. Van Goethem, M. Mertens, and I. F. J. Vankelecom, "Crosslinked PVDF membranes for aqueous and extreme pH nanofiltration," *J. Memb. Sci.*, vol. 572, pp. 489–495, 2019, doi: 10.1016/j.memsci.2018.11.036.